Acta Oceanol. Sin., 2015, Vol. 34, No. 9, P. 12–22
DOI: 10.1007/s13131-015-0733-5
http://www.hyxb.org.cn
E-mail: hyxbe@263.net

Mesoscale surface circulation and variability of Southern Indian Ocean derived by combining satellite altimetry and drifter observations

BENNY N. Peter[1]*, SHENBAKAVALLI Ranjan[2], MAZLAN Hashim[3], MOHD Nadzri Reba[3], MOHD Razali Mahmud[2]

[1] Department of Coastal and Offshore Engineering, School of Ocean Engineering and Underwater Technology, Kerala University of Fisheries and Ocean Studies, Kochi 682506, India

[2] Department of Geomatic Engineering, Faculty of Geoinformation and Real Estate, University of Technology Malaysia, Johor 81310, Malaysia

[3] Institute of Geospatial Science & Technology, Faculty of Geoinformation and Real Estate, University of Technology Malaysia, Johor 81310, Malaysia

Received 22 August 2014; accepted 3 February 2015

Abstract

High resoultion Eulerian mean velocity field has been derived by combining the satellite tracked surface drifter data with satellite altimetry and ocean surface winds. The drifter data used in this study includes Argos and surface drifter data from Global Drifter Program. Maps of Sea Level Anomaly (MSLA) weekly files with a resolution of (1/3)° in both Latitude and Longitude for the period 1993–2012 have been used. The Ekman current is computed using ocean surface mean wind fields from scatterometers onboard ERS 1/2, Quikscat and ASCAT. The derived mean velocity field exhibits the broad flow of Antarctic Circumpolar Current with speeds up to 0.6 m/s. Anomalous field is quite significant in the western part between 20° and 40°E and in the eastern part between 80°E and 100°E with velocity anomaly up to 0.3 m/s. The estimated mean flow pattern well agrees with the dynamic topography derived from *in-situ* observations. Also, the derived velocity field is consistent with the *in-situ* ADCP current measurements. Eddy kinetic energy illustrates an increasing trend during 1993–2008 and is in phase coherence with the Southern Annular Mode by three month lag. Periodic modulations are found in the eddy kinetic energy due the low frequency Antarctic Circumpolar Wave propagation.

Key words: Antarctic Ocean, circulation, satellite altimetry, eddy kinetic energy, Southern Indian Ocean, antarctic circumpolar wave

Citation: Benny N. Peter, Shenbakavalli Ranjan, Mazlan Hashim, Mohd Nadzri Reba, Mohd Razali Mahmud. 2015. Mesoscale surface circulation and variability of Southern Indian Ocean derived by combining satellite altimetry and drifter observations. Acta Oceanologica Sinica, 34(9): 12–22, doi: 10.1007/s13131-015-0733-5

1 Introduction

Over the past two decades, the Southern (Antarctic) Ocean has received much attention as it is playing a crucial role in the global climate system. The circulation of the Antarctic Ocean is mainly comprised of the broad eastward flowing Antarctic Circumpolar Current (ACC) which connects the three major Oceans (Atlantic, Indian and Pacific oceans) and serves as a principal pathway of exchange between these basins and controls the distribution of heat, salt, momentum and nutrients. Hence, the changes occurring in any part of the ocean due to climate forcing are transmitted around the globe through the circumpolar current.

The ACC consists of a number of relatively narrow and deep reaching jets associated with the baroclinic shear (Nowlin and Klinck, 1986) and flows between 45° and 55°S, zonally uninterrupted (Orsi et al., 1995). It is also composed of a series of hydrographic fronts with strong horizontal gradients in potential temperature, salinity and density, implying intense geostrophic currents (Deacon, 1937; Nowlin et al., 1977; Belkin and Gordon, 1996; Moore et al., 1999). North of ACC is the subtropical Convergence or Subtropical Front (STF), usually found between 35° and 40°S. Three fronts and three zones south of STF and associated with the ACC are, from north to south; the Subantarctic Zone (SAZ), the Subantarctic Front (SAF), the Polar Frontal Zone (PFZ), the Polar Front (PF), the Antarctic Zone (AZ), and the Southern ACC Front associated with the southern boundary between the ACC and subpolar regime (Orsi et al., 1995).

ACC transports more water than any other current in the ocean (Klinck and Nowland, 2001) and the average transport is about 135×10^6 m^3/s. Several researchers have estimated the transport (e.g., Nowlin et al., 1977; Bryden and Pillsbury, 1977; Peterson, 1988) of ACC using hydrographic data and direct current measurements. The ACC transport vary in response to changes in the Southern Annular Mode (SAM) (Thompson and Wallace, 2000) and are found to be correlated with the SAM down to seasonal time scales (Meredith et al., 2004; Meredith et al., 2011).

The Antarctic Ocean ventilates the largest volume of the ocean interior (Ganachaud and Wunsch, 2000), and is the primary conduit of exchange between the three major ocean

*Corresponding author, E-mail: bennynpeter@gmail.com

basins (Lumpkin and Speer, 2007). Recent developments suggest that mesoscale eddies playing a prominent role in the dynamics of the Antarctic Ocean (Ito et al., 2010; Hallberg and Gnanadesikan, 2006; Böning et al., 2008).

The satellite data analysis has revealed the presence of the Antarctic Circumpolar wave (ACW), which propagates eastward with the ACC, at a slower rate than the mean flow. The presence of this circumpolar wave has been detected in atmospheric temperature (AT), sea surface temperature (SST), seaice, sealevel pressure (SLP) and mean wind stress (White and Peterson, 1996; Peterson and White, 1998; Cai and Baines, 2001; Park et al., 2004). Though the ACW is closely linked with the ACC, the circumpolar nature of the ACW is not yet clear. Jin (1997) pointed out that the ACW is a result of coupled instability of the ACC and overlying atmosphere. A clear eastward propagation of the ACW was found during the period 1985–1995 (Connolly, 2003).

The ACW encircles the earth every eight to nine years (White and Peterson, 1996). It has a long wave length (wave number equals 2) resulting in two crests and two troughs at any given time. The troughs and crests are associated with massive patches or pools of warm and cold waters respectively. The warm patches are 2 to 3°C warmer than the mean surface temperature (SST) and cold patches are 2 to 3°C colder than the mean SST (White and Peterson, 1996) and directly influence the temperature of the overlying atmosphere. Using a coupled atmosphere and ocean model, Christoph et al. (1998) found that wavenumber 3 is the dominant pattern around the Antarctic, while the wavenumber 2 pattern occurs only in about 20% of the cases. The wavenumber 3 pattern was also identified as the dominant pattern in other models (e.g., Cai et al., 1999). Other analyses indicate that the ACW might have inter-decadal variations (Connolley, 2003; Venegas, 2003).

Among the three major oceans, the Indian Ocean is not extended to the higher latitudes of northern hemisphere whereas, it has a wide opening to the Antarctic Ocean and also connected to the Pacific Ocean through the narrow Indonesian Passage in the tropics. Hence, the oceanic and atmospheric circulation of the Indian Ocean is significantly influenced by the Antarctic Ocean. The deep circulation as well as the water characteristics of the Indian Ocean much depends on the processes taking place in the circumpolar region and the intrusion of thermocline waters through the Indonesian Throughflow (Gordon, 1986). Jacobs and Georgi (1977), Sharma and Peter (1990), and Benny and Sharma (1992) discussed the circulation and transports of Indian sector of Antarctic Ocean from hydrographic observations. The inter-oceanic exchanges of heat and fresh water between Indian and Antarctic oceans were given by Georgi and Toole (1982). Park et al., (1991) carried out a detailed hydrographic survey in the vicinity of Crozet-Kerguelen Islands. Swart et al. (2008) have determined the ACC transport south of Africa and Rintoul et al. (2002) have estimated it for south of Australia.

Climate forcing analysis shows no significant influence of ENSO in the Indian sector. SAM explains up to 20% of the high frequency movement of the Subantarctic Front (SAF) and Polar Front (PF). High frequency positive SAM events are associated with a southward meandering of the fronts (Sallée et al., 2008). Sea level variability with spatial scale of 1 000 km and time scales of 20 days to one year has been found in South Indian Basin (Fukumori et al., 1998; Fu, 2003). A positive correlation exists between ACC fronts location and zero wind stress curl in the southern Indian Ocean (Sallée et al., 2008). A coherence analysis by Dong et al. (2006) suggests that meridional shifts of the PF correspond to the meridional shifts of the wind field.

The surface circulation of Southern Ocean and associated processes are influenced by the high frequency variations (SAM) and low frequency climate modes. The generation of mesosacle eddies and an associated kinetic energy transfer is essentially controlling the air-sea exchanges and climate variability. In order to understand these mesoscale processes a fine resolution surface velocity field is crucial. Hence, the focus of this paper is to derive a high resolution ((1/3)°×(1/3)°) mean surface velocity field of the Southern Indian Ocean and to identify the mesoscale features of surface circulation and its variability using remote sensing observations. The rest of this paper is organised as follows: Section 2 describes the data and method, Section 3 discusses the surface circulation, Section 4 explains the Eddy Kinetic Energy (EKE) distribution and conclusions are given in Section 5.

2 Data and methods

2.1 *Data used*

We used satellite altimetry, satellite tracked surface drifter observations, ocean surface wind observations, Acoustic Doppler Current Profiler (ADCP) observations and hydrographic data. The study area is confined between 20°–120°E and 30°–70°S. The satellite altimeter data used in this study are delayed mode, "Ref" Maps of Sea Level Anomaly (MSLA) produced by the Collect Localisation Satellites (CLS), France (http://www.aviso.altimetry.fr/). The Maps of Sea Level Anomaly were obtained by merging JASON/ TOPEX/POSEIDON and European Remote Sensing Satellites ERS / Envisat data using optimum interpolation (AVISO, 1997). The data set is in weekly format on a (1/3)°×(1/3)° Mercator grid and covers the period 1993–2012.

The surface drifter data used in this study is from the Global Drifter Program (Surface Velocity Program), with the positions of freely drifting buoys located using the ARGOS satellite system. The distribution of drifter tracks (Fig. 1) enables reliable estimate of the velocity field up to 60°S. Data used were quality controlled and optimally interpolated to uniform six-hour interval trajectories using the drifters' position data. This data set is compiled and maintained by the Drifter Data Centre at the Atlantic Oceanographic and Meteorological Laboratory of the National Oceanic and Atmospheric Administration, USA (http://www.aoml.noaa.gov/).

The weekly ocean surface mean wind fields (0.5°×0.5° resolution) produced by the Centre ERS d'Archivage et de Traitement (French) (CERSAT) (http://cersat.ifremer.fr/) at the French Research Institute for Exploration of the Sea (IFREMER) have also been used to separate the wind-driven component from the drifter velocity. The product is derived from the measurements with scatterometers on board the European Space Agency satellites on ERS 1/2 (1993–1999), QuikSCAT (2000–2009) and ASCAT (2010–2012).

The best copy dataset of salinity–temperature profiles of Global Temperature–Salinity Profile Program, obtained from National Oceanographic Data Centre have also been used to determine the dynamic topography.

2.2 *Method*

The surface drifter and altimeter data have been combined to estimate the mean surface velocity (Uchida and Imawaki, 2003; Benny et al., 2014) in this study. At a location x and time t, the

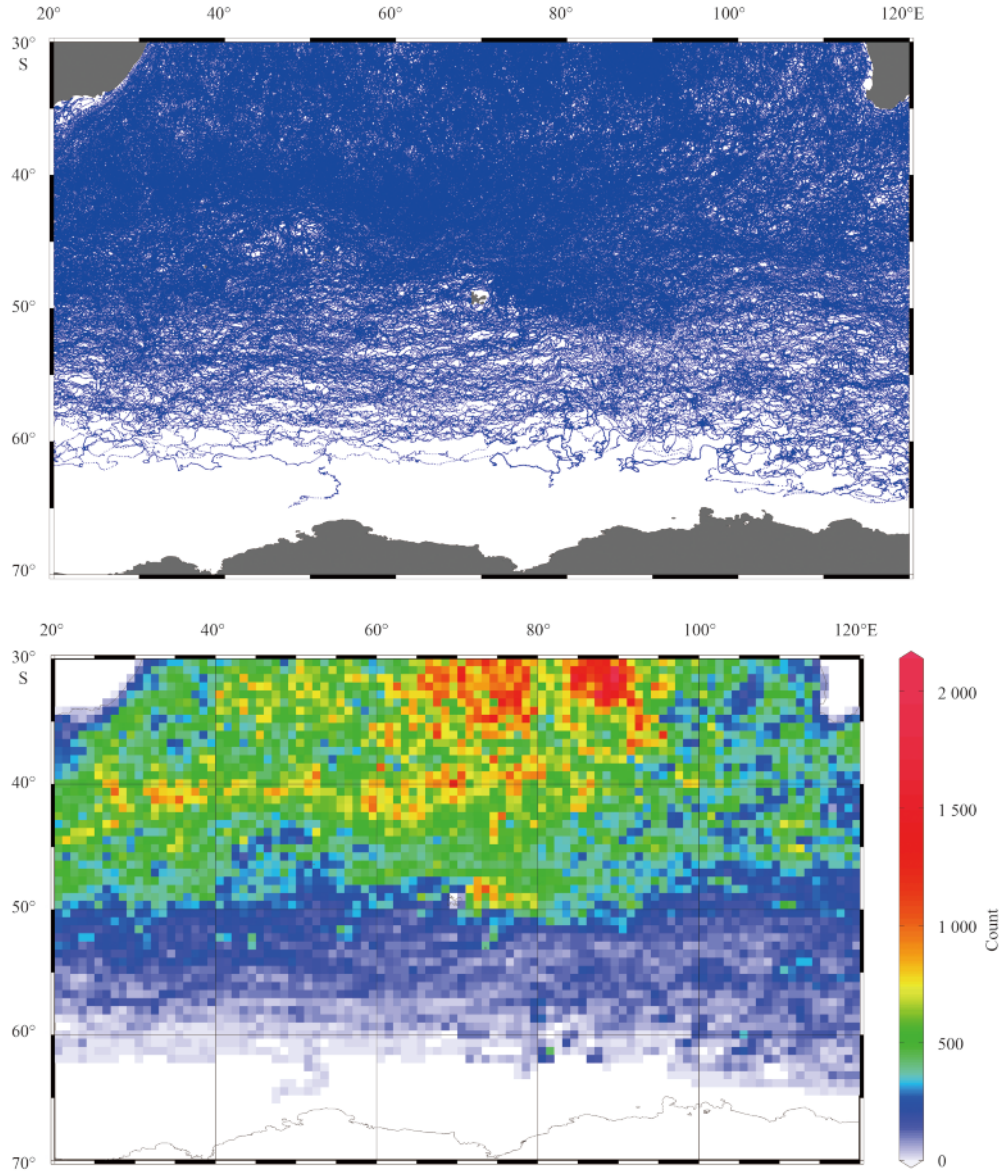

Fig. 1. Available Drifter data tracks during 1993–2012 (upper panel) and drifter data density distriburtion (1993–2012) (lower panel).

instantaneous geostrophic velocity $V_g(x, t)$ can be represented as

$$V_g(x,t) = V_{mg}(x) + V_g'(x,t) , \quad (1)$$

where $V_{mg}(x)$ is the mean geostrophic velocity, $V_g'(x, t)$ is the geostrophic velocity anomaly, i.e.,

$$V_{mg}(x) = V_g(x,t) - V_g'(x,t). \quad (2)$$

The instantaneous geostrophic velocity can be derived from the drifter observations and the altimeter sea level anomalies provide the anomaly field. Hence, the mean velocity is calculated by subtracting the altimeter derived geostrophic velocity anomaly from the drifter-derived geostrophic velocity measured at the same time and location. This method estimates almost unbiased Eulerian mean velocities which are free from the sampling tendency of the drifters. Thus, the unknown mean velocity can be estimated for the grid box where a drifter had passed. The average of the calculated mean velocities in each grid, $<V_{mg}(x)>$ gives a more accurate estimate by reducing the estimation error. In this study, we have estimated mean velocities at locations, wherever five or more drifter observations are available.

The components of geostrophic velocity anomaly have been computed from altimeter sea level anomaly data using the conventional geostrophic relation.

$$u' = -\frac{g}{f}\frac{\partial h}{\partial y} , \quad (3)$$

$$v' = \frac{g}{f}\frac{\partial h}{\partial x} . \quad (4)$$

To remove high frequency fluctuations, the drifter trajectories have been low-pass filtered by a 60–h running mean. Then, the drifter data has been gridded into (1/3)°×(1/3)° latitude×longitude boxes of altimeter observations. The surface velocity has been estimated from the drifter position data in each grid. The

wind-produced slip has been corrected employing the relation given by Niiler and Paduan (1995). An additional correction has been made for drifters which had lost its drogues during its traverse, using the empirical relation given by Pazan and Niiler (2001). The Ekman velocity has been estimated employing the Ralph and Niiler (1999) model as

$$V_E = A \cdot |f|^{-1/2} \cdot W\exp(i \cdot \theta), \quad (5)$$

where $V_E = U_E + iV_E$, is the Ekman current at 15 m depth, A=7×10^{-7} s$^{-1/2}$, f is the coriolis parameter, W is the wind speed, exp (i·θ) (θ=±54) represents the rotation of the Ekman current to the right (left) of the wind vector in the northern (southern) hemisphere.

The geostrophic velocity component has been separated from the drifter velocity by subtracting the Ekman component. The time series maps of instantaneous geostrophic velocity field can be obtained by combining the weekly/monthly maps of sea level anomaly with the estimated mean velocity field.

The mesoscale variability is analysed by determining the Eddy Kinetic Energy (EKE) from the anomalous velocity filed. The EKE is estimated using the components of geostrophic velocity anomaly as

$$EKE = 1/2\left[(u')^2 + (v')^2\right]. \quad (6)$$

3 Surface circulation

3.1 *Mean velocity field*

The mean velocity field (Fig. 2a) estimated by combining the satellite altimetry and drifter observations well illustrates the surface circulation pattern of the Southern Indian Ocean. The eastward flowing ACC is located between 45° and 60°S with speeds mostly below 0.5 m/s. Slight increase in speed (up to 0.75 m/s) is found between 80° and 100°E, where the component of Agulhas Return Current (ARC) merges with the ACC. The south westward flowing Agulhas Current retroflects when it reaches the southern tip of Africa, one part continues to the Atlantic and the rest flow south eastward as ARC. Agulhas Current and its Return Current are visible with high speeds and embedded with eddies and meanders in the mean velocity field. The axis of ARC is inclined west to southeast and it merges with the ACC at around 80°E. The confluence of ACC with ARC enhances the circumpolar flow between 80° and 120°E and the ACC is wider compared to the western part. The ARC is between 39° and 41°S at 20°E and is meandering equatorward up to 37°S at 40°E.

The flow pattern obtained is in good agreement with the Hydrographic Atlas of the Southern Ocean (HASO) (Olbers et al., 1992) and the average surface velocity field from the Fine Resolution Antarctic Model (FARM) Atlas (Webb et al., 1991). The Agulhas and ARC are visible with high velocities and the ACC shows multicore structure associated with the fronts and filaments (Fig. 2b). Based on year-long observations Lutjeharms and Valentine (1984) confirmed that the mean location of the STF as 42°S and ARF (Agulhas Return Front) is between 39° and 40°S in the Southern Indian Ocean.

Previous studies (Read and Pollard, 1993; Orsi et al., 1995) have found SAF and PF merged into a single frontal structure south of Africa. But, Belkin and Gordon (1996) suggest that SAF is a separate feature. Our results do not show individual frontal structure of SAF and PF in the flow field south of Africa at 20°E, but it is evident at 30°E as two cores along 48° and 52°S with speeds 0.40 m/s. The SAF is not clearly identified in FARM Atlas south of Africa (Sparrow et al., 1996) whereas several small, jet like structures are displayed between 50° and 60°S as in our flow pattern at 20°E. Our map also suggests that the SAF is merging

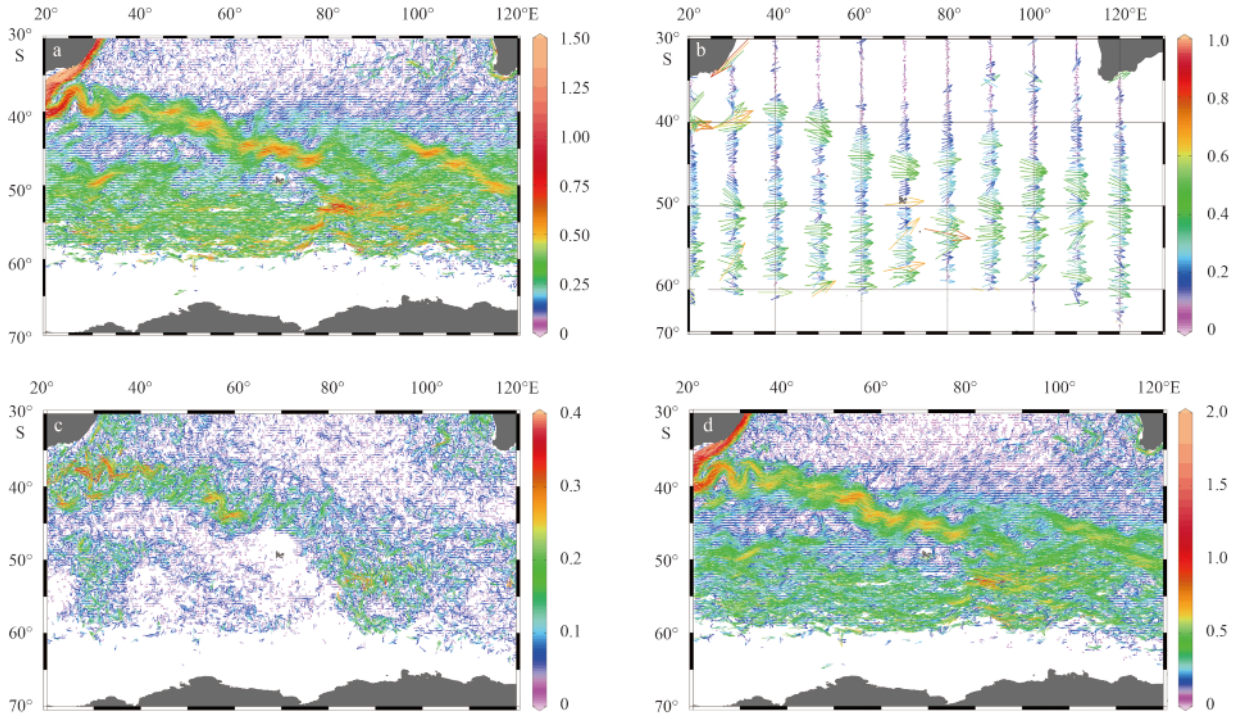

Fig. 2. Mean velocity field estimated by combining satellite altimetry and surface drifter data (m/s) (a), detailed view of mean currents at different longitudes (b)(color represents speed ,m/s), averages of altimeter derived velocity anomalies used for mean field estimation (m/s) (c), and simple averages of drifter derived geostrophic velocity field (m/s) (d).

with the ARF/STF between 50° and 60°E, upstream of Kerguelen Plateau and is flowing as a strong single band with speed around 0.5 m/s. In HASO the SAF have merged with the ARF/STF at 40°E and in FARM it is at 41.4°E. The merging of flow cores is commencing around 40°E but is well defined only from 50°E eastward in our results. The gap between the current cores decreases from 40°E and it became as a single band by 50°E. The flow core associated with PF is also slightly weakened in the longitudinal band 35°–45°E. The southern Jet flow that found around 62°S in FARM and 58°S in HASO respectively is identified around 58°–60°S between 40° and 60°E bands in our map.

In the longitudinal band 50°–60°E, the current cores are slightly shifted southward. The confluence of ARC/STF/SAF is at around 45°S, marked with maximum velocity of 0.5 m/s and the PF core is around 52°S and the southern core is more southward at around 60°S. Park et al. (1993) found that ACC core forms a concentrated jet embedded within a narrow band of the frontal zone, formed by the confluence of STF and SAFs. The confluence results from the northward deflection of the ACC as it crosses Crozet Plateau and the subsequent merging with the ARC. He derived current velocities up to 0.95 m/s from *in-situ* measurements. In the vicinity of the fronts, eastward jets flow approximately two to three times the speed of the current found between them (Klinck and Nowland, 2001).

Along 60°E, the flow pattern shows almost uniform (0.4 m/s) strong current between 40° and 60°S except a weak field around 50°S upstream of Kerguelen Plateau. Between 60° and 80°E the ACC have the maximum surface speeds up to 0.8 m/s. Homogeneous current pattern with respect to latitude is again found at 90° E with less number of current cores. But, many cores appear in the longitudinal band 100°–110°E. More or less latitudinal homogeneity is again attained along 120°E, south of Australia.

The anomaly field (Fig. 2c) shows large velocity variations along the ARC region and between 80° and 100°E, where, the anomaly is up to 0.3 m/s. Significant variance is also observed between 20° and 40°E and the anomaly field is weak between 40° and 80°E in the Antarctic Zone. The large variance in the Antarctic Zone in the eastern region is related to the changes in the ARC.

The absolute current field obtained from the drifter (Fig. 2d) shows strong Agulhas Current and its return flow (up to 2 m/s). The circumpolar current is also strong and its main core is around 50°S at 20°E, but is slightly shifted towards south at 80°E and towards north in the eastern part. Only a minor part of the ARC is turning to subtropical gyre while major part is contributing to the circumpolar flow.

3.2 *Mean dynamic topography*

The mean velocity field estimated by combining the satellite altimetry and drifter observations is compared with the dynamic topography estimated from hydrographic data with reference to 1 000×10^4 Pa. The dynamic topography shows a close similarity with the mean velocity field (Fig. 3). The gradient of steric height clearly depicts the circumpolar flow features. High anomaly around 80°E is visible with high speeds in the velocity map. Also the strong gradient around 50°S along 20°E coincides with the core of the ACC.

3.3 *In-situ ADCP observations and derived velocity filed*

We have made visual comparison of the derived velocity by combining surface drifter and altimeter observations with *in-situ* ADCP observations collected during WOCE period (Cruise No. 0179). The ADCP observations used are along two longitudinal tracks between 80°–120°E and 30°–60°S, the left track covered in December 1994 and the right one in January 1995 (Fig. 4). The absolute velocity field corresponding to the period of ADCP is estimated and compared. The overall flow pattern estimated is well agreeing with *in-situ* measurements. The major flow of the ACC is found between 50° and 55°S and the maximum speed of 0.8 m/s is at around 53°S in the ADCP current distribution. The derived velocity field also depicts strong flow of ACC at the same latitudes with similar speeds. Both velocity fields confirm that significant flow of ACC is taking place between 42° and 57°S in this region.

The velocity section at 115°E (right panel) also shows very similar distribution between observed and estimated fields. The maximum current speed of 0.8 m/s is at around 48°S in both observed and estimated fields. Notably, the core of the ACC flow is shifted more into the lower latitudes between 45° and 50°S. But, significant current flow is occurring between 45° and 60°S. Thus, the spatial variability of ACC is obvious from the *in-situ* measurements as well as in the estimated filed.

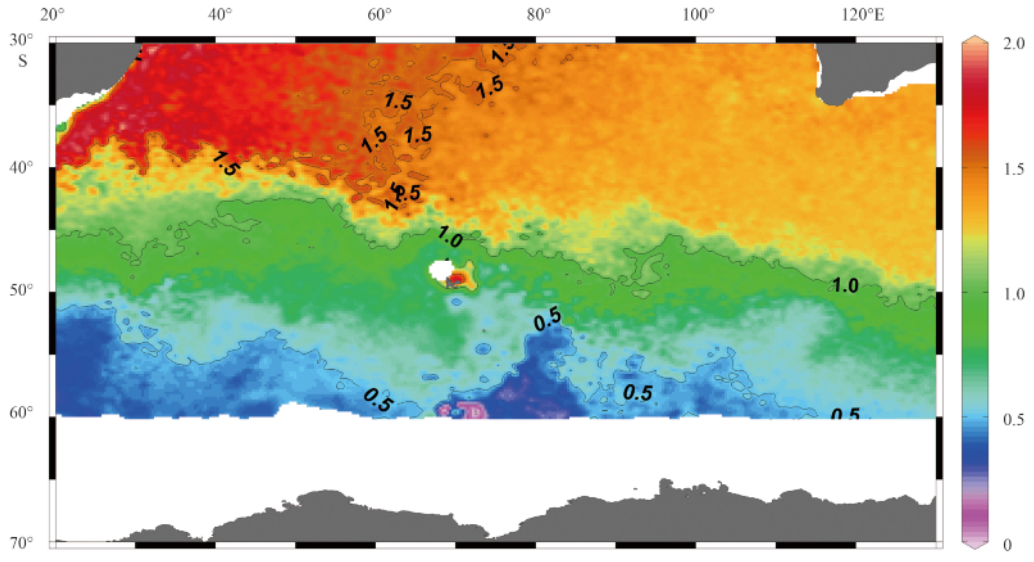

Fig. 3. Mean dynamic height distribution with reference to 1 000×10^4 Pa (dynamic metres).

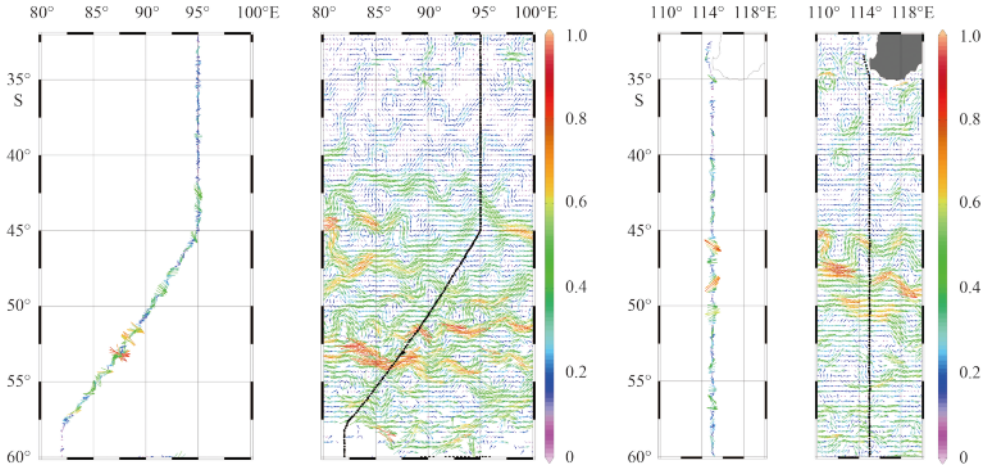

Fig. 4. Comparison with *in-situ* ADCP velocity and velocity estimated combining drifter and altimeter observations (m/s).

3.4 *Zonal current distribution*

In order to understand the seasonal variations of eastward flowing ACC, the average (1993–2008) zonal velocity component during January, April, July and October at 20°, 80° and 120°E have been compared (Fig. 5). The zonal velocity distribution shows no significant seasonal variation specifically, between 50°S and Antarctica, except at 120°E where slight changes are noticed. At 20°E, between Africa and Antarctica the zonal current is very stable compared to the other two sections. Conspicuous seasonal variability (0.1 m/s) is found at 80°E in the northern part between 40° and 50°S where the ARC is merging with the Circumpolar Current. Seasonal variability is also dominant between 45° and 55°S along 120°E section between Australia and Antarctica.

Spatial variability of the ACC is obviously visible in the zonal current distribution. Interestingly, the ACC is more evenly distributed at 20°E, whereas, at 80° and 120°E an odd pattern with number of current cores are found. The Agulhas Current shows westward speed up to 0.6 m/s in January and 0.5 m/s in July and the current core is almost at the same location at 38°S. The ARC is around 41°S with the maximum speed in July and the minimum in October. Between 43° and 55°S the zonal current speed is below 0.25 m/s and two current cores with speeds just above 0.25 m/s are found at 55° and 57°S respectively. Beyond 58°S towards Antarctica the current speed is decreasing and weak westward flow is found at the southern end of the section.

Spatial distribution of zonal velocity at 80°E shows significant deviations from 20°E section. An uneven velocity distribution with number of flow cores are observed between 40° and 60°S. The highest velocity core is at around 54°S with speed up to 0.8 m/s without significant seasonal changes. Another core of flow is at 52°S and has speed above 0.6 m/s. Meanwhile, weak flows prevail around 58° and 49°S, where the zonal speeds are even reduced to zero. In the Subantarctic zone the zonal current is weak (less than 0.3 m/s) except at 44°E, where the current flows at 0.5 m/s. Notably, the zonal current is not showing any significant seasonal variation at 80°E.

As at 80°E, the zonal current is showing an uneven distribution with respect to latitude at 120°E. The southern and northern part of the section illustrates westward flow and between 38°S and 60°S eastward flow prevails. Multicore flow structure is visible in the circumpolar flow and the strongest core is at around 51°S, where the speed is 0.5 m/s in April. Slight seasonal variation is evident in the Antarctic zone in this section.

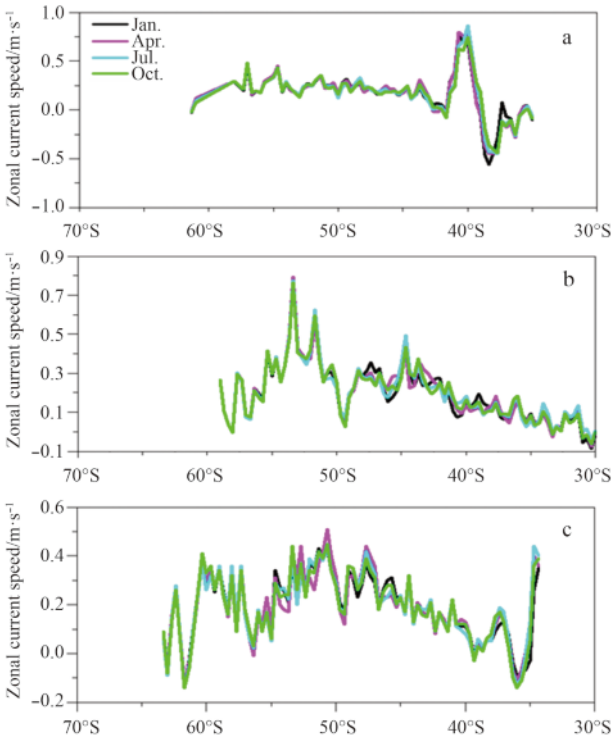

Fig. 5. Zonal current speed distribution at 20°E (a), 80°E (b), and 120°E (c).

The analysis of eastward velocity distribution along various longitudes reveals the seasonal stability of the ACC. But, the ACC shows significant deviations in its structure during its zonal traverse in the Indian sector and is related to the bottom topography. The seasonal climatology estimated invariably display the multicore structure of the ACC at different longitudes which is much stronger in the eastern part of the Indian sector. The multiple jets observed are a robust characteristic of the ACC and is found in number of data sets including repeat hydrographic sections (Sokolov and Rintoul, 2007), repeat acoustic Doppler Current Profiler transects (Firing et al., 2011), sea surface temperature data (Hughes and Ash, 2001) and dynamic heights derived from surface drifters (Niiler et al., 2003; Hughes, 2005). The cur-

rent branches are observed to merge and diverge along the circumpolar path and vary with time (Rintoul and Naveira Garaboto, 2013). Slight seasonal variations found in the eastern part is related to the seasonal changes of the ARC.

4 Eddy kinetic energy (EKE)

Eddy kinetic energy is calculated using the velocity anomaly components to determine the mesoscale variability occurring in the Southern Indian Ocean. The mean (1993–2008) EKE ranges between 0–0.1 m^2/s^2 and maximum is found along the ARC region (Fig. 6). Higher EKE is also visible in the Antarctic zone in the region 20°–40°E and 80°–100°E specifically along 50°S.

The trend of monthly average of EKE of the study region during 1993–2008 (Fig. 7) clearly reveals the Semi-annual Antarctic Oscillation (SAO) as well as the inter-annual variations. Inter-annual variations in SAO strength represent the dominant mode of Southern Hemisphere circulation variability (Connolley, 1997); observation and modelling studies revealed SAO variability on interannual to decadal time scales (Simmonds and Walland, 1997).

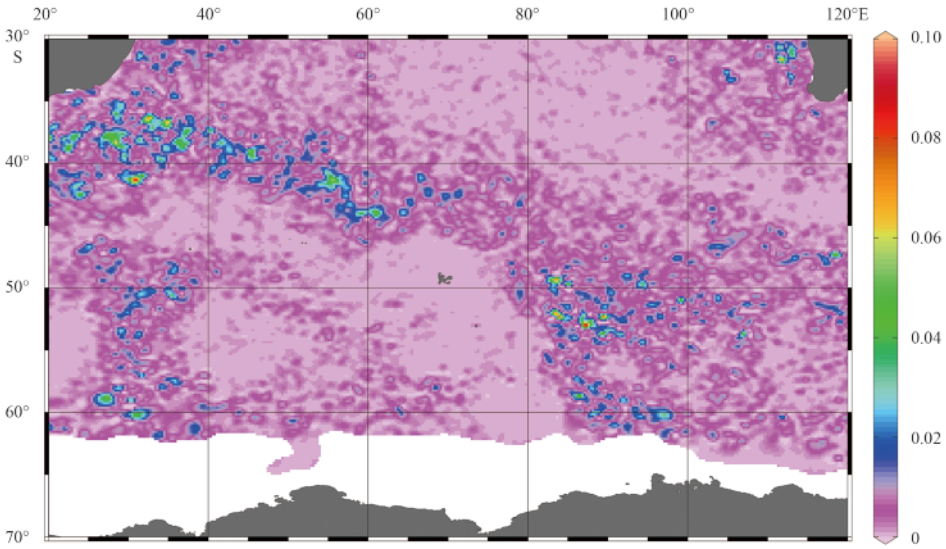

Fig. 6. Distribution of average (1993–2012) EKE (m^2/ s^2).

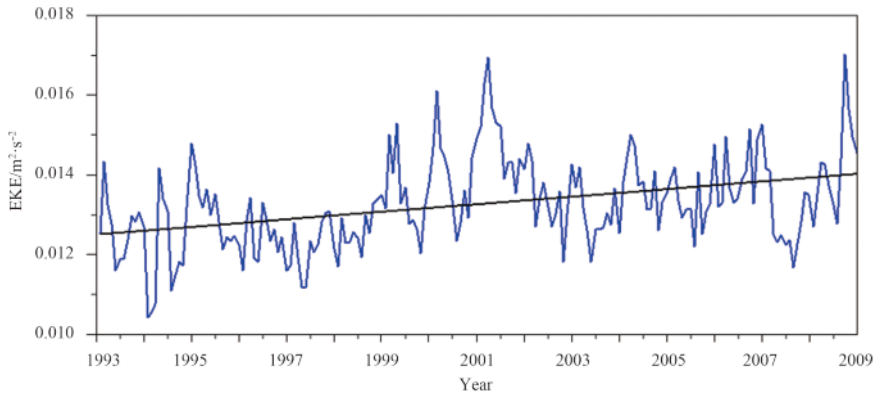

Fig. 7. Time series of EKE during 1993–2008.

Comparison of EKE distribution with SAM index time series from Nan and Li (2003) clearly displays a negative correlation, but, the pattern with 3 months lag (Fig. 8) in EKE shows phase coherence with SAM index excluding periodic influences from the low frequency climate modes, specifically during 2000–2001 period. A characteristic time delay is found in the EKE response to a wind perturbation (Morrow et al., 2010). During positive SAM period, the mid-latitude high pressure shifts more into the higher latitudes that strengthen the westerly wind and develops potential energy anomalies which enhance the northward Ekman drift in the circumpolar region. This result in increased Ekman convergence in the Subtropics and divergence in the polar region and this develops large meridional gradients and tilt in the isopycanls and accelerate the ACC. Thus, the meridional wind variability is essentially imparting baroclinic instability and the eddy activities within a reasonable time scale of about three months.

Overall, a net increasing trend is found in EKE during 1993–2008 period. The increase in EKE trend is in coherence with the net increase in sea level in the Southern Ocean (Lombard et al., 2005) and the increased trend in SAM (Thompson and Wallace, 2000). Morrow et al. (2010) shows that even though SAM induces a coherent forcing that is in phase around the circumpolar band, the ocean's EKE response is different in each basin as eddy generation depends on local interactions between wind stress, topography and mean state. The increase in EKE occur sooner in the Indo-Pacific and EKE response is largest in the Pacific compared to other sectors of the Antarctic Ocean.

The monthly trend of EKE shows low during 1998 and high in 2001. Hence, to identify the spatial variation pattern, we have presented EKE distribution of April (highest peak in 2001) of both years (Fig. 9). Significant increase in EKE is found along the ARC region and southwest of Australia in 2001 and rest of the region shows almost same distribution. The variation in the ARC is due to the energy transmitted through the Rossby wave activity in the lower latitudes of south Indian Ocean (Benny and Mizuno, 2000). The eddy variability southwest of Australia is related to the Leeuwin Current variations.

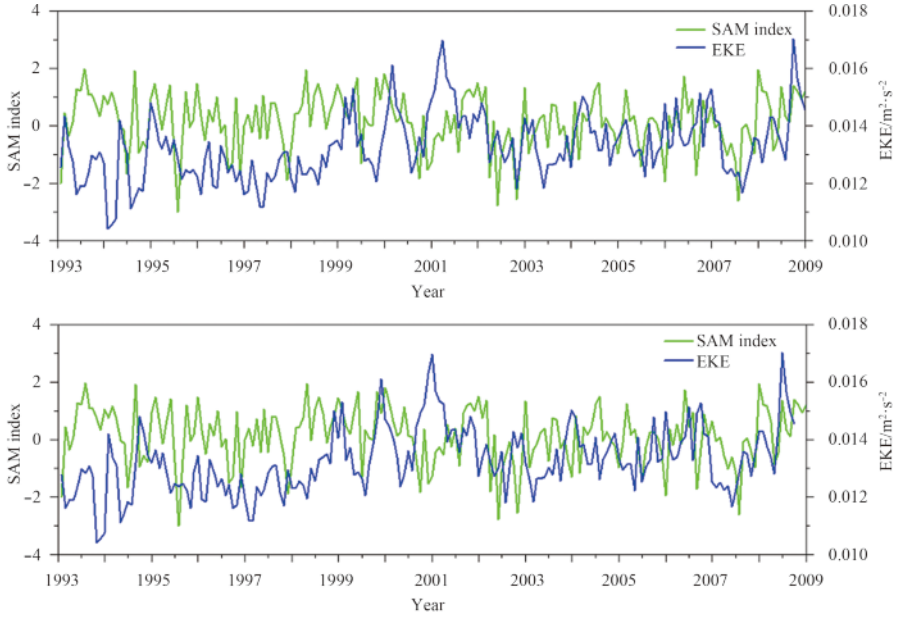

Fig. 8. Monthly average SAM Index and EKE (upper panel) and monthly average SAM Index and EKE (three month lag) (lower panel).

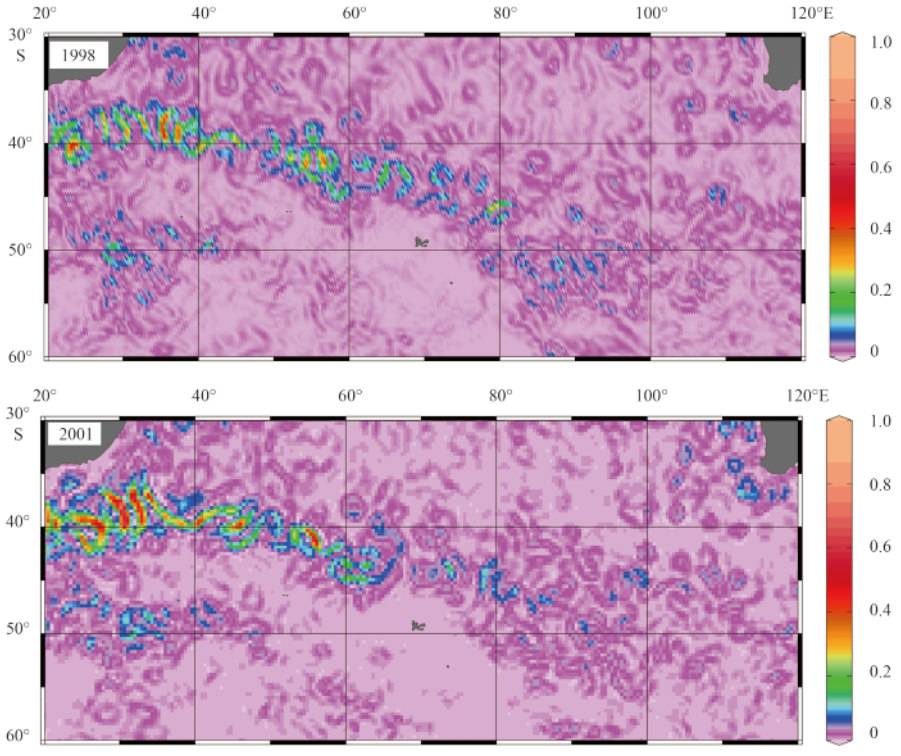

Fig. 9. EKE (m^2/s^2) distribution during April in 1998 and 2001 .

The inter-annual variation of EKE along 52°S between 20° and 120°E in the ACC region during 16 years (1993–2008) is shown in Fig. 10. The unusual increase at around 9th year (1999–2001) compared to its mean indicates the influence of ACW. The ACW propagation in the Indian sector is inferred from Hovmoller plots of SLA and EKE along 52°S (Fig. 11). The SLA field shows west-

east propagation signals, which are clearly discernible only in the region up to 60°E. Three ACW signals during 1994–1995, 2000–2001 and 2004–2005 are found and among which the strongest one is during 2000–2001. Remarkably, the propagation is not organised in the eastern part of the Indian Ocean. The unorganised nature of the ACW propagation in the ice-ocean-atmosphere system of the Indian Ocean sector has been noticed in a few studies (Nuncio et al., 2011; White and Annis, 2004; Gloersen and White, 2001). The weakening in eastward propagating anomaly may be due to the meandering of ACC and associated surface current variations and heat fluxes (Nuncio et al., 2011). Earlier studies (Peterson and White, 1998; White and Annis, 2004) show that ACW branches northward in the Indian Ocean sector, and reaches the Indonesian Seas and continues its circuit around the globe.

The Hovmoller plot of EKE also supports the propagation of

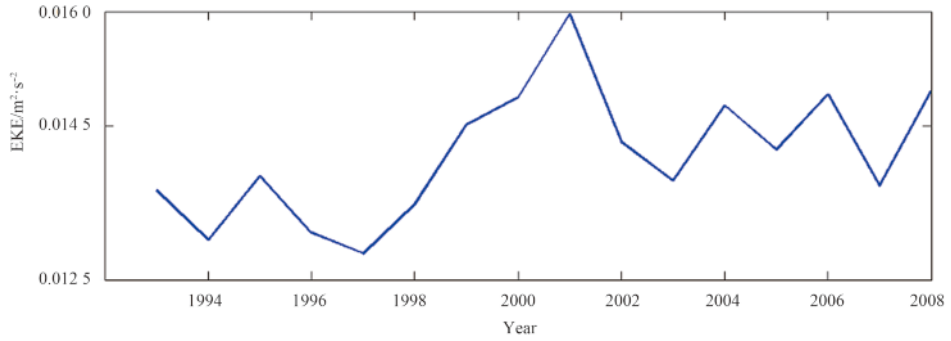

Fig. 10. Inter-annual variation of EKE along 52°S during 1993–2008.

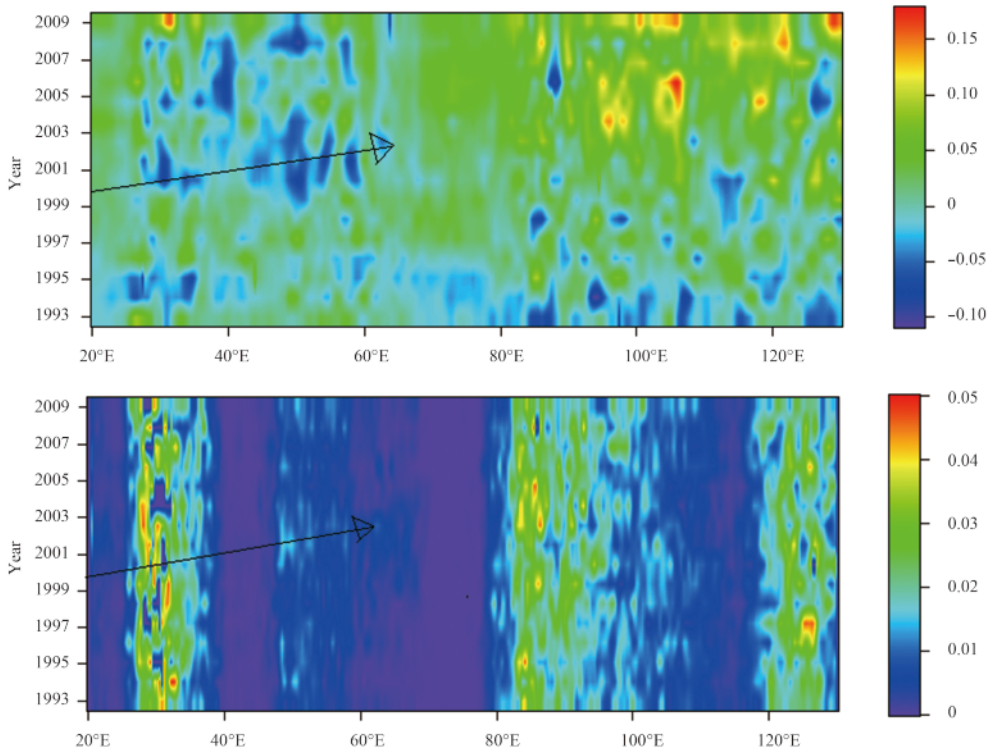

Fig. 11. Hovmoller Plot of SLA (m) along 52°S (upper panel) and Hovmoller Plot of EKE (m^2/s^2) along 52°S (lower panel).

ACW during the same periods and strong anomalies observed during 2000–2001 period. Thus, the abnormal increase in EKE during 1999–2001 coincides with the propagation of the strongest ACW during the period. White et al. (1998) describes the ACW as a self-organisation with-in the global ocean-atmosphere system that requires the spherical shape of the rotating earth for its propagation and mean meridional temperature gradient for its maintenance. There are many theories regarding the origin of ACW and the 4–5 year periodicity observed in the ACW links it with ENSO (White and Peterson, 1996; Peterson and White, 1998; Cai and Baines, 2001; Park et al., 2004). The geostrophic balance between low and high pressure centres gives rise to poleward/equatorward flows resulting in the surface atmosphere temperature anomalies, which in turn induces SST anomalies by direct warming/cooling as a result of reduced or enhanced fluxes (Venegas, 2003).

Thus, the EKE distribution reveals seasonal to inter-annual variation in the Southern Ocean. Models and observations sug-

gest that the ACC responds to an increase in wind forcing primarily by increasing EKE rather than increasing transport (Tansley and Marshall, 2001; Hallberg and Gnanadesikan, 2006; Meredith and Hogg, 2006; Munday et al., 2013). Stronger wind forcing increases the baroclinicity of the ACC; baroclinic instability then releases available potential energy and increases the EKE, regaining the pre-perturbation baroclinic state. The degree of topographic blocking will also influence the eddy kinetic energy and even relatively small eddies can make up a significant percentage of the current's overall eddy kinetic energy (Knauss, 1996).

5 Conclusions

Combining satellite altimetry and surface drifter observations the present study brings out mesoscale circulation features of the Southern Indian Ocean. The mean velocity field obviously illustrates the ACC, ARC and traces of westward coastal current near Antarctic Coast. The anomaly field is strong in the ARC region and in the Antarctic Zone between 80° and 100°E. The ACC shows significant spatial variation and slight seasonal changes mainly in the subantarctic region and attains maximum zonal speed in the central region between 70° and 100°E. The EKE distribution shows maximum mesoscale variability in the ARC region and also significant variability between 80° and 100°E in the Antarctic Zone. The monthly EKE shows an increasing trend in the Indian Ocean region during 1993–2008 and illustrates a semi-annual oscillation as well as the modulations by SAM and ACW. Significant inter-annual variability is occurring mainly along ARC region and southwest of Australia. An organised propagation of ACW is clearly visible in the western part of the Indian sector of the Circumpolar Ocean. The periodic modulation of eddy kinetic energy in the Southern Indian Ocean is related to the passage of ACW. The changes in EKE is mostly consistent with SAM index by three month lag except the years with ACW influence.

Acknowledgements

The author acknowledges financial support for the work from UTM GUP Antarctic research grant Vote No. Q.J130000. 2409.01G27, MOHE. We used altimeter data set produced by the Collect Localisation Satellites, Space Oceanography Division as part of Environment and Climate. Drifter data produced by the National Oceanic and Atmospheric Administration, Atlantic Oceanographic and Meteorological Laboratory are utilized. Also employed the wind data set produced and provided by the French Processing and Archiving Facility (CERSAT) at the French Research Institute for Exploration of the Sea. The hydrographic data used is from NODC, Washington. We used ODV, Schlitzer R, Ocean Data View, http://odv.awi.de, 2013, for preparing graphics.

References

Archiving, Validation, Interpretation of Satellite Oceanographic Data (AVISO). 1997. In: AVISO Handbook: Sea Level Anomaly Files, 21st ed, France, 24

Belkin I M, Gordon A L. 1996. Southern ocean fronts from the greenwich meridian to Tasmania. J Geophys Res, 101(C2): 3675–3696

Benny N P, Ambe D, Mridula K R, et al. 2014. Mean and seasonal circulation of the south Indian Ocean estimated by combining satellite altimetry and surface drifter observations. Terrestrial, Atmospheric and Oceanic Sciences, 25(1): 91–106

Benny N P , Mizuno K. 2000. Annual cycle of steric height in the Indian Ocean estimated from the thermal field. Deep Sea Research Part I: Oceanographic Research Papers, 47(7): 1351–1368

Benny N P, Sharma G S. 1992. Circulation in the Indian Ocean region of the Antarctica Ocean. Proc Indian Natn Sci Acad, 58(2): 155–172

Böning C W, Dispert A, Visbeck M, et al. 2008. The response of the Antarctic circumpolar current to recent climate change. Nature Geoscience, 1: 864–869

Bryden H L, Dale Pillsbury R. 1977. Variability of deep flow in the drake passage from year-long current measurements. J Phys Oceanogr, 7(6): 803–810

Cai Wenju, Baines P G, Gordon H B. 1999. Southern mid- to high-latitude variability, a zonal wavenumber-3 pattern, and the Antarctic circumpolar wave in the CSIRO coupled model. J Climate, 12(10): 3087–3104

Cai Wenju, Baines P G. 2001. Forcing of Antarctic circumpolar wave by El Nino-Southern Oscillation teleconnections. J Geophys Res, 106(C5): 9019–9038

Christoph M, Barnett T P, Roeckner E. 1998. The Antarctic circumpolar wave in a coupled ocean-atmosphere GCM. J Climate, 11(7): 1659–1672

Connolley W M. 1997. Variability in annual mean circulation in southern high latitudes. Clim Dyn, 13(10): 745–756

Connolley W M. 2003. Long-term variation of the Antarctic Circumpolar Wave. J Geophys Res, 107(C4): 8076

Deacon G E R. 1937. The hydrology of the southern ocean. Discovery Reports, 15: 3–122

Dong Shenfu, Sprintall J, Gille S T. 2006. Location of the Antarctic polar front from AMSR-E satellite sea surface temperature measurements. J Phys Oceanogr, 36(11): 2075–2089

Firing Y L, Chereskin T K, Mazloff M R. 2011. Vertical structure and transport of the Antarctic Circumpolar Current in Drake Passage from direct velocity observations. J Geophys Res, 116(C8): C08015

Fu L L. 2003. Wind-forced intraseasonal sea level variability of the extratropical oceans. J Phys Oceanogr, 33(2): 436–449

Fukumori I, Raghunath R, Fu L L. 1998. Nature of global large-scale sea level variability in relation to atmospheric forcing: A modeling study. J Geophys Res, 103(C3): 5493–5512

Ganachaud A, Wunsch C. 2000. Improved estimates of global ocean circulation, heat transport and mixing from hydrographic data. Nature, 408(6811): 453–457

Georgi D T, Toole J M. 1982. Antarctic circumpolar current and oceanic heat and freshwater budgets. J Mar Res, 40: 183–197

Gloersen P, White W B. 2001. Reestablishing the circumpolar wave in sea ice Antarctica from one winter to the next. J Geophys Res, 106(C3): 4391–4395

Gordon A L. 1986. Interocean exchange of thermocline water. J Geophys Res, 91(C4): 5037–5046

Hallberg R, Gnanadesikan A. 2006. The role of eddies in determining the structure and response of the wind-driven southern hemisphere overturning: results from the modeling eddies in the southern ocean (MESO) project. Journal of Physical Oceanography, 36(12): 2232–2252

Hughes C W, Ash E R. 2001. Eddy forcing of the mean flow in the Southern Ocean. J Geophys Res, 106(C2): 2713–2722

Hughes C W. 2005. Nonlinear vorticity balance of the Antarctic Circumpolar Current. J Geophys Res, 110(C11): C11008

Ito T, Woloszyn M, Mazloff M. 2010. Anthropogenic carbon dioxide transport in the southern ocean driven by ekman flow. Nature, 463(7277): 80–83

Jacobs S S, Georgi D T. 1977. Observations on the southwest Indian/Antarctic Ocean. In: Angel M, ed. A voyage of Discovery. Oxford: Pergamon Press, 43–84

Jin Feifei. 1997. A theory of interdecadal climate variability of the North Pacific ocean-atmosphere system. J Climate, 10(8): 1821–1835

Klinck J M, Nowland W D Jr. 2001. Antarctic Circumpolar Current. Encyclopedia of Ocean Science. New York: Academic Press, 151–159

Knauss J A. 1996. Introduction to Physical Oceanography. Prentice-Hall, Inc., 152–162

Lombard A, Cazenave A, Traon P Y L, et al. 2005. Contribution of thermal expansion to present-day sea-level change revisited.

Global and Planetary Change, 47(1): 1–16
Lumpkin R, Speer K. 2007. Global ocean meridional overturning. Journal of Physical Oceanography, 37(10): 2550–2562
Lutjeharms J R E, Valentine H R. 1984. Southern ocean thermal fronts south of Africa. Deep-Sea Research Part A: Oceanographic Research Papers, 31(12): 1461–1475
Meredith M P, Hogg A M. 2006. Circumpolar response of Southern Ocean eddy activity to a change in the Southern Annular Mode. Geophys Res Lett, 33(16): L16608
Meredith M P, Woodworth P L, Chereskin T K, et al. 2011. Sustained monitoring of the Southern Ocean at Drake Passage: past achievements and future priorities. Reviews of Geophysics, 49(4): RG4005
Meredith M P, Woodworth P L, Hughes C W, et al. 2004. Changes in the ocean transport through drake passage during the 1980s and 1990s, forced by changes in the southern annular mode. Geophys Res Lett, 31(21): L21305
Moore J K, Abbott M R, Richman J G. 1999. Location and dynamics of the Antarctic polar Front from satellite sea surface temperature data. J Geophys Res, 104(C2): 3059–3073
Morrow R, Ward M L, Hogg A M, et al. 2010. Eddy response to Southern Ocean climate modes. J Geophys Res, 115(C10): C10030
Munday D R, Johnson H L, Marshall D P. 2013. Eddy saturation of equilibrated circumpolar currents. J Phys Oceanogr, 43(3): 507–532
Nan Sulan, Li Jianping. 2003. The relationship between the summer precipitation in the Yangtze River valley and the boreal spring Southern Hemisphere Annular Mode. Geophys Res Lett, 30(24): 2266
Niiler P P, Paduan J D. 1995. Wind-driven motions in the Northeast Pacific as measured by Lagrangian drifters. J Phys Oceanogr, 25(11): 2819–2830
Niiler P P, Maximenko N A, McWilliams J C. 2003. Dynamically balanced absolute sea level of the global ocean derived from near-surface velocity observations. Geophys Res Lett, 30(22): 2164
Nowlin W D Jr, Klinck J M. 1986. The physics of the Antarctic circumpolar current. Rev Geophys, 24(3): 469–491
Nowlin W D Jr, Whitworth T III, Pillsbury R D. 1977. Structure and transport of the antarctic circumpolar current at drake passage from short-term measurements. J Phys Oceanogr, 7(6): 788–802
Nuncio M, Luis A J, Yuan X, et al. 2011. Topographic meandering of Antarctic Circumpolar Current and Antarctic Circumpolar Wave in the ice-ocean-atmosphere system. Geophysical Research Letters, 38(13): L13708
Olbers D, Gouretski V, Seiß G, et al. 1992. Hydrographic Atlas of the Southern Ocean. Bremerhaven, Germany: Alfred Wegener Institute for Polar and Marine Research, 17
Orsi A H, Nowlin W D Jr, Whitworth T II. 1993. On the circulation and stratification of the Weddell Gyre. Deep Sea Research Part I: Oceanographic Research Papers, 40(1): 169–203
Orsi A H, Whitworth T III, Nowlin W D Jr. 1995. On the meridional extent and fronts of the Antarctic circumpolar current. Deep-Sea Research Part I, 42(5): 641–673
Park Y H, Gambéroni L, Charriaud E. 1991. Frontal structure and transport of the Antarctic Circumpolar Current in the south Indian Ocean sector, 40–80°E. Mar Chem, 35(1–4): 45–62
Park Y H, Gamberoni L, Charriaud E. 1993. Frontal structure,water masses, and circulation in the Crozet Basin. J Geophys Res, 98(C7):12361–12385
Park Y H, Roquet F, Vivier F. 2004. Quasi-stationary ENSO wave signals versus the Antarctic Circumpolar Wave scenario. Geophys Res Letts, 31(9): L09315
Pazan S E, Niiler P P. 2001. Recovery of near-surface velocity from undrogued drifters. J Atmos Oceanic Technol, 18: 476–489
Peterson R G. 1988. On the transport of the Antarctic circumpolar current through drake passage and its relation to wind. J Geophys Res, 93(C11): 13993–14004
Peterson R G, White W B. 1998. Slow oceanic teleconnections linking the Antarctic Circumpolar Wave with the tropical El Nino-Southern Oscillation. J Geophys Res, 103(C11): 24573–24583
Ralph E A, Niiler P P. 1999. Wind-driven currents in the tropical Pacific. J Phys Oceanogr, 29(9): 2121–2129
Read J F, Pollard R T. 1993. Structure and transport of the Antarctic Circumpolar Current and Agulhas Return Current at 40°E. J Geophys Res, 98(C7): 12281–12295
Rintoul S R, Sokolov S, Church J. 2002. A 6 year record of baroclinic transport variability of the Antarctic Circumpolar Current at 140°E derived from expendable bathythermograph and altimeter measurements. J Geophys Res, 107(C10): 3155
Rintoul S R, Naveira Garabato A C. 2013. Dynamics of the southern ocean circulation. In: Siedler G, Griffies S M, Gould J, et al., eds. Ocean Circulation and Climate: A 21st Century Perspective. Oxford, GB: Academic Press, 471–492
Sallée J B, Speer K, Morrow R. 2008. Response of the Antarctic Circumpolar Current to atmospheric variability. J Climate, 21(12): 3020–3039
Sharma G S, Peter B N. 1990. Entrainment of circumpolar water in the Indian Ocean region of the Antarctic. Proc Indian Acad Sci, 99(3): 425–438
Simmonds I, Walland D J. 1997. Decadal and centennial variability of the southern semiannual oscillation simulated in the GFDL coupled GCM. Clim Dyn, 14(1): 45–53
Sokolov S, Rintoul S R. 2007. Multiple jets of the Antarctic circumpolar current south of Australia. J Phys Oceanogr, 37(5): 1394–1412
Sparrow M D, Heywood K J, Brown J, et al. 1996. Current structure of the south Indian Ocean. Journal of Geophysical Research: Oceans, 101(C3): 6377–6391
Swart S, Speich S, Ansorge I J, et al. 2008. Transport and variability of the Antarctic circumpolar current south of Africa. J Geophys Res, 113(C9): C09014
Tansley C E, Marshall D P. 2001. Flow past a cylinder on a plane, with application to Gulf Stream separation and the Antarctic Circumpolar Current. J Phys Oceanogr, 31(11): 3274–3283
Thompson D W J, Wallace J M. 2000. Annular modes in the extratropical circulation. Part I: month-to-month variability. J Climate, 13(5): 1000–1016
Uchida H, Imawaki S. 2003. Eulerian mean surface velocity field derived by combining drifter and satellite altimeter data. Geophysical Research Letters, 30(5): 1229
Venegas S A. 2003. The Antarctic circumpolar wave: A combination of two signals? J Climate, 16: 2509–2525
Webb D J, Killworth P D, Coward A C, et al. 1991. The FRAM Atlas of the Southern Ocean. Swindon: Natural Environment Research Council, 67
White B W, Peterson R G. 1996. An Antarctic circumpolar wave in surface pressure, wind, temperature and sea-ice extent. Nature, 380(6576): 699–702
White B W, Chen S C, Peterson R G. 1998. The Antarctic Circumpolar Wave: A beta effect in ocean-atmosphere coupling over Southern Hemisphere. J Phys Oceanogr, 28(12): 2345–2361
White W B, Annis J. 2004. Influence of the Antarctic circumpolar wave on El Niño and its multidecadal changes from 1950 to 2001. J Geophys Res, 109(C6): C06019